American Mineralogist, Volume 95, pages 1305–1311, 2010

Toturite $Ca_3Sn_2Fe_2SiO_{12}$—A new mineral species of the garnet group

Irina O. Galuskina,[1,*] Evgeny V. Galuskin,[1] Piotr Dzierżanowski,[2] Viktor M. Gazeev,[3] Krystian Prusik,[4] Nikolai N. Pertsev,[3] Antoni Winiarski,[5] Aleksandr E. Zadov,[6] and Roman Wrzalik[5]

[1]Faculty of Earth Sciences, Department of Geochemistry, Mineralogy and Petrography, University of Silesia, Będzińska 60, 41-200 Sosnowiec, Poland
[2]Institute of Geochemistry, Mineralogy and Petrology, Warsaw University, al. Żwirki i Wigury 93, 02-089 Warszawa, Poland
[3]Institute of Geology of Ore Deposits, Petrography, Mineralogy and Geochemistry (IGEM), Russian Academy of Sciences, Staromonetny 35, 119017 Moscow, Russia
[4]Faculty of Materials Science, University of Silesia, Bankowa 9, 40-007 Katowice, Poland
[5]August Chełkowski Institute of Physics, University of Silesia, Uniwersytecka 4, 40-007 Katowice, Poland
[6]OOO Science-Research Center NEOCHEM, Dmitrovskoye Highway 100/2, 127238 Moscow, Russia

Abstract

A new Sn-rich garnet, toturite $Ca_3Sn_2Fe_2SiO_{12}$, occurs as an accessory mineral in high-temperature altered carbonate-silicate xenoliths in ignimbrite of the Upper Chegem structure in the Northern Caucasus, Kabardino-Balkaria, Russia. The empirical formula of toturite from the holotype sample is $(Ca_{2.989}Fe^{2+}_{0.011})_{\Sigma 3}(Sn^{4+}_{1.463}Sb^{5+}_{0.325}Ti^{4+}_{0.193}Zr_{0.013}Mg_{0.003}Nb^{5+}_{0.002}Cr_{0.001})_{\Sigma 2}(Fe^{3+}_{1.633}Al_{0.609}Si_{0.552}Ti^{4+}_{0.166}Fe^{2+}_{0.039}V^{5+}_{0.001})_{\Sigma 3}O_{12}$. The mineral forms thin regular growth zones and irregular spots in the Fe^{3+}-dominant analog of kimzeyite. Toturite is cubic, $Ia\bar{3}d$, $a \approx 12.55$ Å, as is confirmed by electron backscatter diffraction (EBSD) data. The strongest lines of the calculated powder diffraction pattern are [*d*, Å (*hkl*) *I*]: 2.562 (422) 100, 1.677 (642) 91, 3.138 (400) 74, 4.437 (220) 67, 1.146 (10.4.2) 31, 1.046 (884) 25, 1.984 (620) 23. Raman spectra of toturite are analogous to those of kimzeyite and shows the following diagnostic bands (cm^{-1}): 244, 301, 494, 497, 575, 734. The association of toturite with larnite, rondorfite, wadalite, magnesioferrite, lakargiite, and cuspidine indicates a high temperature (>800 °C) of formation. The mineral name is given after the Totur River situated in Eltyubyu village, also Totur is the name of a Balkarian god.

Keywords: Garnet, toturite, Fe^{3+}-dominant analog of kimzeyite, Sn, Sb, Raman spectroscopy, EBSD, Lakargi Mountain, Russia

Introduction

Toturite, $Ca_3Sn_2Fe^{3+}_2SiO_{12}$, is a structural analog of kimzeyite ($Ca_3Zr_2Al_2SiO_{12}$) and schorlomite ($Ca_3Ti_2Fe^{3+}_2SiO_{12}$). It was discovered in altered carbonate-silicate xenoliths from ignimbrites of the Upper Chegem caldera, Kabardino-Balkaria, Russia. Unusual compositions of garnet from the altered xenoliths are represented by the complex solid solution $Ca_3(Sn,Zr,Ti^{4+},Sb^{5+},U^{6+}...)_2(Fe^{3+},Al,Si,Fe^{2+},Ti^{4+}...)_3O_{12}$ in which SnO_2 content reaches 38.51 wt%. For determination of the toturite end-member formula the dominant valence rule by Hatert and Burke (2008) was used, which considered a coupled heterovalent substitution at the octahedral (Y) and tetrahedral (Z) sites of garnet structure.

Several new minerals have been discovered in the xenoliths near Lakargi Mountain: calcio-olivine γ-Ca_2SiO_4 (Zadov et al. 2008), lakargiite $CaZrO_3$ (Galuskin et al. 2008), chegemite $Ca_7(SiO_4)_3(OH)_2$ (Galuskin et al. 2009), kumtyubeite $Ca_5(SiO_4)_2F_2$ (Galuskina et al. 2009), $KNa_2Li(Mg,Fe)_2Ti_2Si_8O_{24}$ (IMA2009-009), and $CaUO_4$ (IMA2002-032). Other new garnet species from these xenoliths were also recently approved. These are elbrusite-(Zr) $Ca_3U^{6+}ZrFe^{3+}_2Fe^{2+}O_{12}$ (Galuskina et al. 2010b), bitikleite-(SnAl) $Ca_3Sb^{5+}SnAl_3O_{12}$, and bitikleite-(ZrFe) $Ca_3Sb^{5+}ZrFe^{3+}_3O_{12}$ (Galuskina et al. 2010a). These garnet species form solid solutions with toturite. A more widespread garnet in altered xenoliths in the area of Lakargi Mountain, and that also forms a solid solution with toturite, is $Ca_3Zr_2Fe^{3+}_2SiO_{12}$ (IMA2009-029) originally described from the Kerimasi volcano (Tanzania) recently approved by the CNMNC IMA. This garnet, which is the $^{IV}Fe^{3+}$ analog of kimzeyite $Ca_3Zr_2Al_2SiO_{12}$ (Milton et al. 1961; Munno et al. 1980), has already been described from the kimzeyite type locality at Magnet Cove, U.S.A. (Whittle et al. 2007), and other localities, namely, Anguillara, Italy (Schingaro et al. 2001), and Wiluy, Russia (Galuskina et al. 2005).

Tin in natural garnet has been reported only as a minor constituent in andradite (as SnO_2): 2.9 wt% [Gumble, New South Wales, Australia; Mulholland (1984)]; 3.5 wt% [(El Hamman, Central Morocco; Sonnet (1981)]; 5.8 wt% [Davib Ost, South West Africa; McIver and Mihálik (1975)]; 6.01 wt% [Tyrnyauz, Russia; Kononov et al. (1989)]. Amthauer et al. (1979) suggested that Sn is incorporated in Sn-bearing andradite via $Sn^{4+}+Fe^{2+} = 2Fe^{3+}$.

We did not find in the extensive literature on synthetic garnet any information about the synthesis of the Sn analog of kimzeyite ($Ca_3Sn_2Al_2SiO_{12}$) or its Fe^{3+} analog ($Ca_3Sn_2Fe^{3+}_2SiO_{12}$). Mössbauer investigations of synthetic Y-Sn-garnet $Ca_{3-x}Y_xSn_xFe_{5-x}O_{12}$ for

* E-mail: irina.galuskina@us.edu.pl

$0.1 \le x \le 1.5$ (Belov and Lyubutin 1966) and also $Ca_2YSn_2Fe_3O_{12}$ (Amthauer et al. 1979) point to Sn^{4+} incorporation at the octahedral site, whereas investigations of Ca-Sn-Ga-garnets have shown that Sn may be incorporated at all three structural sites simultaneously (Rulmont et al. 1993, 1995). Artificial Zr-free garnet with 26.26 wt% SnO_2 and an approximate formula $(Ca_{2.92}Mg_{0.08})_{\Sigma3}(Sn_{1.03}Ti_{0.28}Fe^{3+}_{0.54}Fe^{2+}_{0.15})_{\Sigma2}(Si_{1.84}Al_{0.53}Fe^{3+}_{0.63})_{\Sigma3}O_{12}$ has been noted in association with cassiterite in tin-refining slag (Butler 1978).

Toturite (IMA2009-033) was approved by the CNMNC IMA in July 2009. The name is geographical on the one hand and historical on the other. The name is given after the Totur River situated in Eltyubyu village, the starting point for the climb to Lakargi Mountain where the mineral is found. In addition, Totur is the name of a Balkarian god, and an ancient warrior, after whom the local Totur fortress near Tyrny-Auz and the clan tower, Totur-Kale, at Eltyubyu are named. The type sample with toturite crystals is deposited in the collections of the Fersman Mineralogical Museum, Russian Academy of Sciences, specimen number 3839/1.

Experimental methods

The morphology and composition of garnet crystals were investigated using a Philips/FEI ESEM XL30/EDAX scanning electron microscope (Faculty of Earth Sciences, University of Silesia) and a CAMECA SX100 electron-microprobe analyzer with wavelength dispersive spectrometers (Institute of Geochemistry, Mineralogy, and Petrology, University of Warsaw). The composition of the garnet was determined at 15 kV, 40–50 nA using natural and synthetic standards.

The small size of the toturite required the use of single-crystal electron backscatter diffraction (EBSD) analysis. EBSD images were recorded using the HKL EBSD system on the JSM-6480 high-performance scanning electron microscope (Institute of Materials Science, University of Silesia) using 30 kV beam energy. Thin sections used for electron microprobe analyses were re-polished using an Al_2O_3 suspension with a 20 nm particle size. To minimize the charging effect, the specimens were coated by a several tens of nanometers thick carbon layer. The EBSD experiments were performed in the vacuum of 0.1 mPa. The calibration of the EBSD system geometry was carried out on Si single crystal for two detector distances (DD)—177 and 150 mm. The Nordlys II camera with a resolution of 1344×1024 pixels was used. Either 2×2 binning or no binning was applied for the electron backscatter patterns collection at the different DD. To improve the pattern quality long acquisition time between 300–3000 ms were applied. Additionally, frame averaging was used for maximum noise reduction. Depending on the DD and single-pattern collection time, up to 30 frames were averaged. The "Channel5" software package (Oxford Instruments, Day and Trimby 2004) was used for the interpretation of the EBSD patterns. For 150 mm DD, only manual band detection were applied. This is due to the fact that the Hough transformation does not work very well for the high bandwidths. For DD of 177 mm the manual plus Hough (maximum 125 resolution) band detection were applied. In the match 54 reflectors and 7–11 bands were used.

An optimization procedure was applied to estimate the symmetry and cell parameter of toturite. First, an approximate cell parameter was calculated from the electron microprobe analysis at one point (no. 12, Table 1) according to the equation (Strocka et al. 1978): $a = b_1+b_2r_X+b_3r_Y+b_5r_Xr_Y+b_6r_Xr_Z+b_4r_Z$ (Å), where $b_1 = 7.02954$; $b_2 = 3.31277$; $b_3 = 2.49398$; $b_4 = 3.34124$; $b_5 = -0.87758$; $b_6 = -1.38777$ and r_X, r_Y, r_Z = weight-averaged effective ionic radii of cations (Shannon 1976). Then the calculated cell parameter for this point was matched to values calculated from the kimzeyite structure (Munno et al.1980) with Zr replaced by Sn using PowderCell for Windows version 2.4 (Kraus and Nolze 1996). Several structure files were created with the *a* parameter ranging from 12.35 to 12.65 Å. Last, EBSD patterns were fitted with each structure file. It was assumed that the structure giving the best match (minimum MAD) has the actual cell parameter of toturite with the composition at point no. 12 (Table 1).

A powdered sample of polymineral pseudomorph consisting of tazheranite-like phase and garnet was examined with a rotating anode and Ag*K*α radiation at 60 kV and 200 mA on a μXRD D/max RAPID II Rigaku equipped with a *K*α monochromator and curved imaging plate systems for 2D X-ray scattering (August Chełkowski Institute of Physics, University of Silesia). A PowderCell for Windows version 2.4 (Kraus and Nolze 1996), based on the Rietveld method, was used to refine unit-cell dimensions of the garnet and tazheranite-like phase. The same software helped to calculate the theoretical XRD powder pattern of toturite using the model with the best mean angular deviation from EBSD data and cation occupancy from electron-microprobe data.

Raman spectra of single crystals of toturite were recorded using a LabRAM HR800 (Jobin-Yvon-Horiba) equipped with a 1800 line/mm grating monochromator, a charge-coupled device (CCD), Peltier-cooled detector (1024×256), and an Olympus BX40 confocal microscope (Wrocław University of Technology). The incident laser excitation was provided by a water-cooled argon laser source operating at 514.5 nm. The power at the exit of 100× objective lens varied from 40–60 mW. The Raman spectra were recorded in 0° geometry, in the range of 50–4000 cm^{-1} Raman shift and with a spectral resolution of 2.5 cm^{-1}. The collection time was 10 s and 16 scans were accumulated. The monochromator was calibrated using the Raman scattering line of a silicon plate (520.7 cm^{-1}).

Occurrence and description of toturite

Toturite occurs in the high-temperature cuspidine skarn formed at the immediate contact of a carbonate-silicate xenolith with ignimbrite (contact breccia?) near Lakargi Mountain, Upper Chegem caldera, Kabardino-Balkaria, Northern Caucasus, Russia (Gazeev et al. 2006). Toturite forms impregnations in thin (1–10 mm) whitish zones of rock with pseudomorphs after ignimbrite phenocrysts of diopside and biotite in xenolith 3 [numbering after Gazeev et al. (2006); Galuskin et al. (2009)]. Toturite is associated not only with early-stage skarn minerals such as cuspidine, rondorfite, wadalite, larnite, magnesioferrite, ellestadite-OH, lakargiite, Fe^{3+}-dominant analog of kimzeyite, and andradite, but also with their alteration products, e.g., various Ca-hydrosilicates (afwillite, hillebrandite, tobermorite, and others), hydrogarnet of the katoite-hibschite series, hydrocalumite, and minerals of the ettringite group (Fig. 1a).

Toturite is represented by different morphological types distinguished also by their compositions (Figs. 1b–1e; Table 1). Sb-free toturite is confined to the zone adjacent to non-altered ignimbrite. Here, toturite forms complicated pseudomorphs after zircon, the central parts of which are filled with fine mixture of Fe^{3+}-dominant analog of kimzeyite (Table 1, analysis 2), a tazheranite-like phase and lakargiite (Fig. 1b). μXRD-data for the this type of pseudomorph 60×45 μm in size reveal the presence of two main phases, i.e., a garnet with $a = 12.542(1)$ Å and a phase close to tazheranite with a slightly increased parameter $a = 5.150(1)$ Å. Toturite forms thin zones on the pseudomorphs (Table 1, analyses 3 and 4). Here, single inhomogeneous crystals, ca. 10 μm in size, of Sb-free toturite with maximum tin contents occur (Table 1, analysis 5).

A few centimeters from the contact with ignimbrite, Sb-bearing toturite (holotype sample, Table 1, analysis 1) is located in close proximity to cuspidine-larnite veins with a Fe-analog of rondorfite (Fig. 1a). This toturite forms a later zone and/or substitutes for Fe^{3+}-dominant analog of kimzeyite (Figs. 1c–1d; Table 1, analyses 6, 7, 9–13). Epitaxic growths of andradite on early garnet crystals are evident (Table 1, analysis 8). Zoned garnet crystals reach 30 μm in size, but toturite zones are, as a rule, thin and usually do not exceed 3–5 μm (Figs. 1c–1d). Successive zones of toturite and the Fe^{3+}-dominant analog of kimzeyite reflect different generations of garnet (Fig. 1b) and substitution of the unstable central part of the garnet crystal (Figs. 1d–1e).

The small scale of the crystals and of thin zones in complex

TABLE 1. Chemical composition of garnet from cuspidine-hydrogrossular skarn

	1	s.d.	Range	2	3	4	5	6	7	8	9	10	11	12	13
UO_3 wt%	n.d.			0.35	2.76	1.05	1.83	n.d.	0.10	n.d.	n.d.	1.22	n.d.	n.d.	0.10
V_2O_5	0.02	0.03	0–0.08	n.d.	n.d.	n.d.	n.d.	n.d.	n.d.	n.d.	0.06	n.d.	n.d.	n.d.	n.d.
Nb_2O_5	0.03	0.04	0–0.11	n.d.	0.18	0.13	0.18	n.d.	0.10	n.d.	n.d.	0.21	n.d.	0.07	0.13
Sb_2O_5	7.77	0.76	6.55–8.94	0.24	n.d.	0.09	n.d.	7.78	0.12	n.d.	8.03	0.14	6.88	7.33	0.16
SiO_2	4.90	0.32	4.44–5.54	7.42	5.42	6.00	4.95	4.84	9.82	35.11	5.12	8.48	5.54	4.76	9.13
TiO_2	4.24	0.54	2.99–5.01	2.96	4.82	4.97	5.95	4.27	3.31	0.06	2.99	4.30	4.92	4.53	2.87
ZrO_2	0.24	0.52	0–2.35	29.05	11.55	11.78	1.51	0.11	31.22	n.d.	n.d.	27.18	0.16	0.11	31.88
SnO_2	32.58	0.78	30.50–33.83	10.04	25.78	28.13	38.51	32.68	4.24	0.16	33.83	6.80	32.30	32.60	4.96
HfO_2	0.01	0.02	0–0.08	0.62	0.20	0.25	0.08	n.d.	0.68	n.d.	n.d.	0.38	n.d.	n.d.	0.46
ThO_2	n.d.			n.d.	n.d.	n.d.	n.d.	n.d.	0.14	n.d.	n.d.	0.20	n.d.	n.d.	0.38
Al_2O_3	4.59	0.23	4.32–5.23	4.06	4.18	4.83	4.85	4.46	6.51	0.53	4.60	3.78	5.13	4.66	6.77
Sc_2O_3	n.d.			0.35	0.19	0.43	0.46	n.d.	0.32	n.d.	n.d.	0.26	n.d.	n.d.	0.32
Cr_2O_3	0.01	0.01	0–0.04	n.d.	n.d.	n.d.	n.d.	n.d.	0.08	n.d.	n.d.	0.05	n.d.	n.d.	0.04
Fe_2O_3	19.27	0.51	18.33–20.15	17.64	17.25	16.01	15.96	19.44	14.91	30.67	19.02	19.37	19.01	18.99	14.61
FeO	0.53	0.40	0–1.34	0.30	0.48	0.32	0.07	0.39	0.39	n.d.	0.69	0.29	0.04	0.07	0.30
MnO	n.d.			0.04	n.d.	n.d.	0.04	n.d.	n.d.	n.d.	n.d.	n.d.	n.d.	n.d.	n.d.
CaO	24.78	0.35	24.16–25.34	26.23	24.72	25.52	24.98	24.82	27.32	33.03	24.58	26.67	25.26	24.9	27.06
MgO	0.02	0.01	0–0.05	n.d.	0.02	n.d.	n.d.	0.02	n.d.	n.d.	n.d.	n.d.	0.05	n.d.	n.d.
SrO	<0.1			n.d.	n.d.	n.d.	n.d.	n.d.	0.16	n.d.	n.d.	0.14	n.d.	n.d.	0.11
Y_2O_3	<0.1			n.d.	n.d.	n.d.	n.d.	n.d.	n.d.	n.d.	n.d.	0.07	n.d.	n.d.	n.d.
La_2O_3	n.d.			n.d.	n.d.	0.18	n.d.	n.d.	n.d.	n.d.	n.d.	n.d.	n.d.	n.d.	n.d.
Ce_2O_3	n.d.			n.d.	0.20	n.d.	n.d.	n.d.	n.d.	n.d.	n.d.	n.d.	n.d.	n.d.	n.d.
Total	98.99			99.30	97.75	99.69	99.37	98.81	99.42	99.56	98.92	99.54	99.15	98.02	99.28
							Calculated on 8 cations and 12 O atoms								
Ca	2.989			3.001	2.995	3.002	3.016	3.002	2.984	3.004	2.988	2.989	3.000	3.027	2.983
Mn^{2+}				0.004			0.004								
Fe^{2+}	0.011								0.004		0.012				0.001
Sr									0.009			0.008			0.007
Y												0.004			
Th									0.003			0.005			0.009
La^{3+}						0.007									
Ce^{3+}					0.008										
X site	3.000			3.005	3.003	3.009	3.020	3.002	3.000	3.004	3.000	3.006	3.000	3.027	3.000
Sn^{4+}	1.463			0.413	1.164	1.231	1.731	1.470	0.172	0.005	1.530	0.284	1.428	1.475	0.203
Zr	0.013			1.512	0.637	0.631	0.083	0.006	1.552			1.388	0.009	0.006	1.599
Ti^{4+}	0.193				0.093	0.046	0.066	0.193	0.210	0.004	0.132	0.241	0.280	0.179	0.138
Hf				0.019	0.006	0.008	0.003		0.020			0.011			0.014
Sb^{5+}	0.325			0.010		0.004		0.326	0.005		0.338	0.005	0.275	0.309	0.006
Nb	0.002				0.009	0.006	0.009		0.005			0.010		0.004	0.006
U^{6+}				0.008	0.066	0.024	0.043		0.002			0.027			0.002
Sc				0.033	0.019	0.041	0.045		0.028			0.024			0.029
Cr	0.001								0.006			0.004			0.003
Mg	0.003				0.003			0.003					0.008		
Fe^{3+}										1.959					
Al										0.033					
Y site	2.000			1.995	1.997	1.991	1.980	1.998	2.000	2.001	2.000	1.994	2.000	1.973	2.000
Fe^{3+}	1.633			1.418	1.468	1.323	1.353	1.652	1.144		1.624	1.525	1.584	1.622	1.131
Fe^{2+}	0.039			0.027	0.045	0.029	0.007	0.037	0.029		0.053	0.025	0.003	0.007	0.025
Si	0.552			0.792	0.613	0.659	0.558	0.547	1.001	2.980	0.581	0.887	0.613	0.540	0.939
Al	0.609			0.511	0.557	0.625	0.644	0.594	0.782	0.020	0.615	0.466	0.670	0.623	0.821
Ti^{4+}	0.166			0.238	0.317	0.364	0.438	0.170	0.044		0.123	0.097	0.130	0.208	0.084
V^{5+}	0.001										0.004				
Sn^{4+}				0.014											
Z site	3.000			3.000	3.000	3.000	3.000	3.000	3.000	3.000	3.000	3.000	3.000	3.000	3.000

Notes: 1 = Toturite, mean from 21 analyses. 2–4 = Garnet from complex pseudomorph shown in Figure 1b. 2 = Fe^{3+}-dominant analog of kimzeyite. 3, 4 = Toturite. 5 = Single crystal of toturite ca. 11 μm in size with maximum Sn content. 6–8 = Crystal in Figure 1d. 6 = Toturite. 7 = Fe^{3+}-dominant analog of kimzeyite. 8 = Andradite. 9–11 = Crystal in Figure 1e. 9 = Toturite. 10 = Fe^{3+}-dominant analog of kimzeyite. 11 = Toturite. 12, 13 = Zoned crystal used for EBSD analysis, Figure 3b. 12 = Toturite. 13 = Fe^{3+}-dominant analog of kimzeyite. Fe^{2+}/Fe^{3+} was calculated from the charge balance, s.d. = standard deviation.

crystals (usually <10 μm) did not allow determination of many of the physical properties of toturite as required for a new mineral species. Toturite is light-brown or yellow in color. The streak is white with a cream tint. The mineral is optically isotropic. The calculated density (for the composition as given in Table 1, analysis 1) is ~4.49 g/cm^3. Structural data were obtained from a zoned crystal of toturite and the Fe^{3+}-dominant analog of kimzeyite (Fig. 2; Table 1, analyses 12 and 13) using EBSD analysis. The interpretation of these data and modeling of the structure were performed using kimzeyite data (Munno et al. 1980) as the ionic radii of Zr (0.72 Å) and Sn (0.69 Å) are close (Shannon 1976). Kikuchi images of toturite and Fe^{3+}-dominant kimzeyite are very similar (Fig. 3). The Kikuchi image of toturite shows an excellent fit with the kimzeyite type structure with parameter $a \approx 12.55$ Å and MAD = 0.14°. Fitting data obtained for Fe^{3+}-dominant analog of kimzeyite using the same model gave MAD = 0.62° to the larger size of a in toturite compare to kimzeyite, which in turn is due to the higher Si content in kimzeyite. Table 2 gives the calculated diffraction pattern for toturite with $a = 12.55$ Å and a composition corresponding to analysis 12 (Table 1).

Raman spectroscopic data confirm that toturite belongs to the garnet group. Raman spectra of toturite are analogous to those of

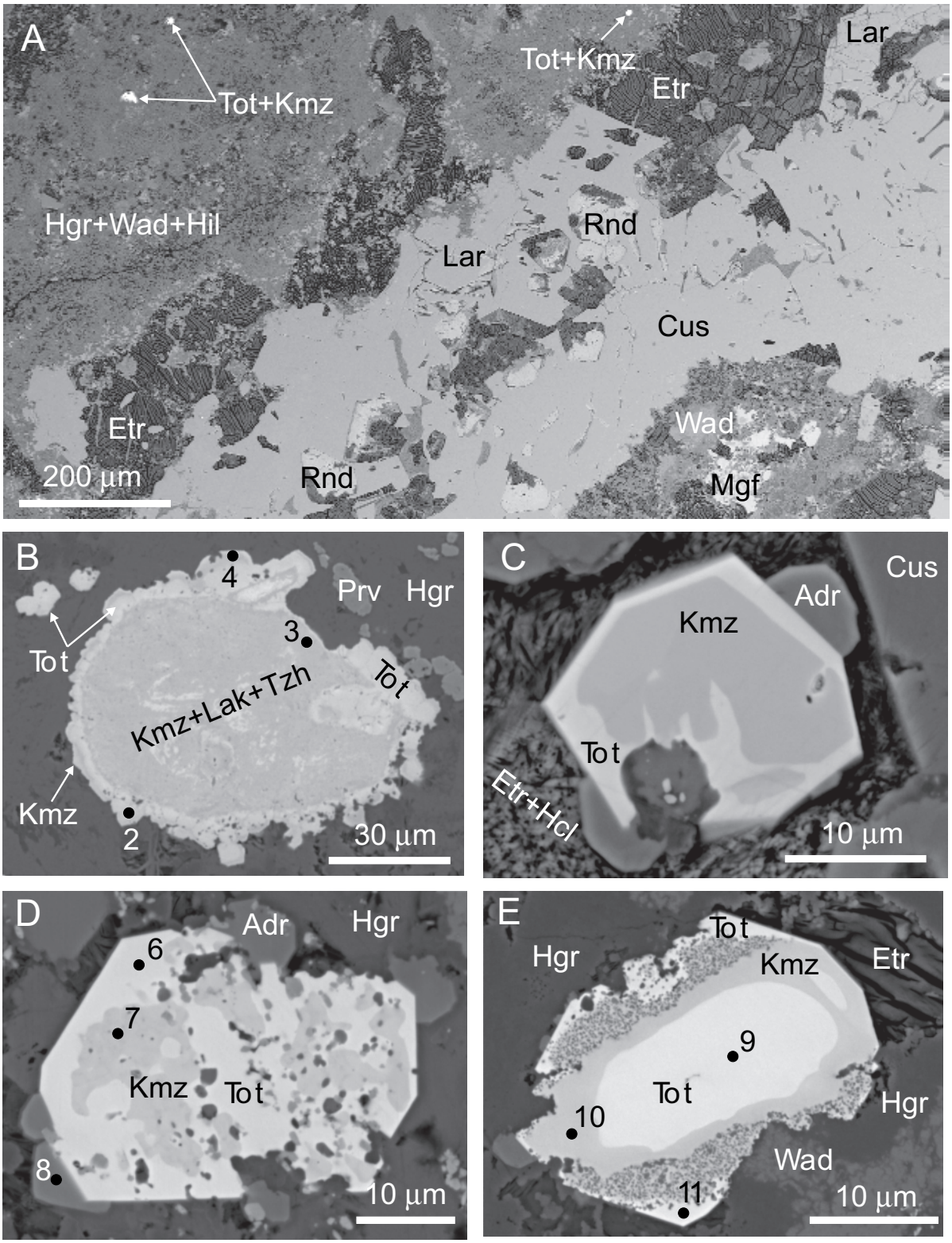

FIGURE 1. (**a**) Cuspidine-hydrogrossular skarn with toturite; (**b**) rim of toturite and the Fe^{3+}-dominant analog of kimzeyite around a complex pseudomorph after zircon; (**c**) {211} crystal of Fe^{3+}-dominant analog of kimzeyite with toturite rim and small epitaxic andradite crystals; (**d**) topotaxic replacement of the Fe^{3+}-dominant analog of kimzeyite by toturite, small dark inclusions = wadalite; (**e**) Fe^{3+}-dominant analog of kimzeyite crystal, in which toturite replaces the central part and forms a later zone. Adr = andradite, Cus = cuspidine, Etr = ettringite group minerals, Hcl = hydrocalumite, Hgr = hibschite-katoite, Hil = hillebrandite, Kmz = Fe^{3+}-dominant analog of kimzeyite, Lak = lakargiite, Lar = larnite, Mgf = magnesioferrite, Rnd = rondorfite, Prv = perovskite, Tot = toturite, Tzh = tazheranite, Wad = wadalite. The numbers correspond to the numbers of analyses in Table 1.

kimzeyite (Schingaro et al. 2001; Galuskina et al. 2005) and are also similar to the spectrum of synthetic garnet $Ca_xSn_xGa_{8-2x}O_{12}$ ($2.5 < x < 3.0$) (Rulmont et al. 1995). The following bands are characteristic of toturite (Fig. 3) (strong bands are bold, cm^{-1}): 148, 156, 185, **244**, 266, **301**, 345, 413, **494**, **497**, 527, **575**, 678, **734**, 784, 810, 879, and 930. That Fe^{3+} is the predominant tetrahedral cation is reflected in the well-displayed band near 734 cm^{-1}. There are no bands in the OH region on the Raman spectra of toturite.

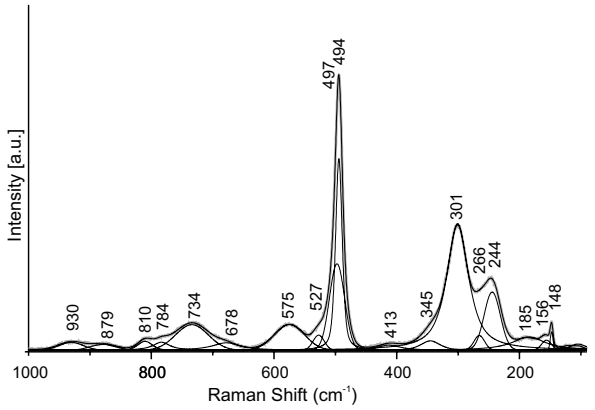

FIGURE 2. Raman spectrum of toturite obtained at point 9 shown in Figure 1e. Gray line = experimental, black line = calculated.

DISCUSSION

Toturite is the end-member of a continuous complex solid solution of Ca-garnet $Ca_3(Sn,Zr,Ti^{4+},Sb^{5+},U^{6+}...)_2(Fe^{3+},Al,Si,Fe^{2+},Ti^{4+}...)_3O_{12}$. The main end-members, some of

TABLE 2. Calculated XRD pattern of toturite (for Co*K*α and Debye-Scherrer geometry)

hkl	*d* (Å$_{cal}$)	I_{cal}	*hkl*	*d* (Å$_{cal}$)	I_{cal}
211	5.124	2	653	1.500	<1
220	4.437	67	822	1.749	7
321	3.354	1	840	1.403	23
400	3.138	74	842	1.369	11
420	2.806	59	664	1.338	19
332	2.676	7	851	1.323	<1
422	2.562	100	844	1.281	5
431	2.461	6	853	1.268	1
521	2.291	2.5	862	1.231	5
440	2.219	5.5	864	1.165	7
532	2.036	4	10.4.2	1.146	31
620	1.984	23	880	1.109	17
640	1.740	19	866	1.076	3
642	1.677	91	884	1.046	25
800	1.569	15.5			

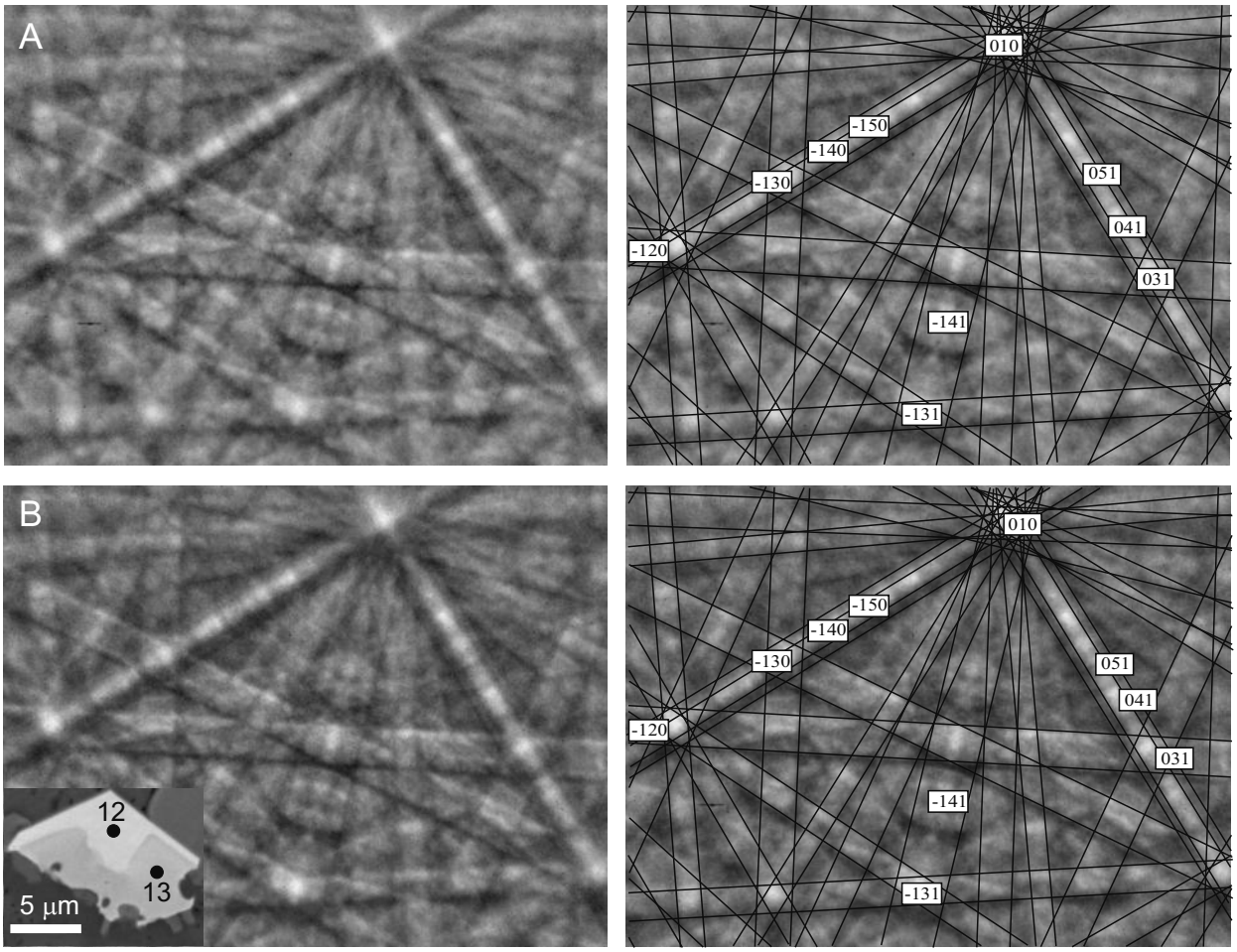

FIGURE 3. Electron backscatter diffraction patterns of a zoned garnet crystal: (**a**) toturite (analysis 12; Table 1), (**b**) Fe^{3+}-dominant analog of kimzeyite (analysis 13; Table 1).

which are not silicates, can be distinguished: $Ca_3Sn_2Fe_2^{3+}SiO_{12}$ (toturite), $Ca_3Zr_2Fe_2^{3+}SiO_{12}$ (Fe^{3+}-dominant analogue of kimzeyite), $Ca_3Zr_2Al_2SiO_{12}$ (kimzeyite), $Ca_3Ti_2^{4+}Fe_2^{3+}SiO_{12}$ (schorlomite), $Ca_3Ti_2^{4+}Al_2SiO_{12}$ (theoretical), $Ca_3Ti_2^{4+}Fe_2^{3+}Ti^{4+}O_{12}$ (theoretical), $Ca_3Ti_2^{4+}Al_2Ti^{4+}O_{12}$ (theoretical), $Ca_3U^{6+}ZrFe_2^{3+}Fe^{2+}O_{12}$ [elbrusite-(Zr)], $Ca_3Sb^{5+}SnAl_3O_{12}$ [bitikleite-(SnAl)], $Ca_3Sb^{5+}ZrFe_3^{3+}O_{12}$ [bitikleite-(ZrFe)], $Ca_3Sn_2Al_2SiO_{12}$ (theoretical), $Ca_3Sn_2Al_2Ti^{4+}O_{12}$ (theoretical), and $Ca_3Sn_2Fe_2^{3+}Ti^{4+}O_{12}$ (theoretical). The calculation of end-member contents for garnet group minerals with such complicated chemical composition is very difficult and not unambiguous (Locock 2008). We used a classification diagram based on the main components, generalized to common crystal-chemical types of garnet: $Ca_3(Zr,Ti^{4+})_2[(Fe^{3+},Al)_2(Si,Ti^{4+})]O_{12}$ (kimzeyite-schorlomite type) – $Ca_3Sn_2[(Fe^{3+},Al)_2(Si,Ti^{4+})]O_{12}$ (toturite type) – $Ca_3[Sb^{5+}(Zr,Sn,Ti^{4+})](Fe^{3+},Al)_3O_{12}$ (bitikleite type) shown in Figure 4. Within every crystal-chemical type, we used the dominant valence rule, considering a coupled heterovalent substitution at the octahedral (Y) and tetrahedral (Z) sites to distinguish garnet species (Hatert and Burke 2008). Complete miscibility between kimzeyite and toturite is evident; as is confirmed by the intermediate compositions of garnet (Fig. 4) in xenolith 5 located a few meters from xenolith 3.

Two compositional types of toturite occur in xenolith 3. The first type, with maximum SnO_2 contents up to 38.5 wt%, shows high Ti^{4+} contents at the tetrahedral site: $(Ca_{3.016}Mn^{2+}_{0.004})_{\Sigma 3.02}(Sn_{1.731}Zr_{0.083}Ti^{4+}_{0.066}Sc_{0.045}U^{6+}_{0.043}Nb_{0.009}Hf_{0.003})_{\Sigma 1.980}(Fe^{3+}_{1.353}Al_{0.644}Si_{0.558}Ti^{4+}_{0.438}Fe^{2+}_{0.007})_{\Sigma 3}O_{12}$ (Table 1, analysis 5). The second type, with high Sb_2O_5 contents up to 9 wt% and SnO_2 contents up to 33.8 wt%, shows decreased $^{IV}Ti^{4+}$ contents: $(Ca_{2.989}Fe^{2+}_{0.011})_{\Sigma 3}(Sn_{1.463}Sb^{5+}_{0.325}Ti^{4+}_{0.193}Zr_{0.013}Mg_{0.003}Nb_{0.002}Cr_{0.001})_{\Sigma 2}(Fe^{3+}_{1.633}Al_{0.609}Si_{0.552}Ti^{4+}_{0.166}Fe^{2+}_{0.039}V^{5+}_{0.001})_{\Sigma 3}O_{12}$ (Table 1, analysis 1). Ti^{4+} is inferred to occupy the tetrahedral site in toturite because the octahedral site is nearly filled by large cations such as Zr, Sn, U^{6+}, and Sc (Table 1). Ti^{4+} at the tetrahedral site was mentioned in natural garnet (Wu and Mu 1986; Scordari et al. 1999; Galuskina et al. 2005; Katerinopoulou et al. 2009). We do not exclude a Sn presence at the tetrahedral site in toturite, as that was noted in synthetic garnet (Geller 1967; Cartié et al. 1992; Rulmont et al. 1993, 1995), but absence of a strong band near 780 cm^{-1} in the Raman spectrum of toturite implies that almost all the Sn is at the octahedral site. Fe^{2+} content calculated from stoichiometry does not exceed 0.1 atom per 8 cations/12 O and, thus, would have little effect on the overall crystal chemistry of toturite. We have assumed that this relatively large cation can be accommodated together with Fe^{3+} at the tetrahedral site. Nonetheless, these ambiguities in site assignments in toturite could be resolved only when we have a crystal suitable for XRD single-crystal investigations.

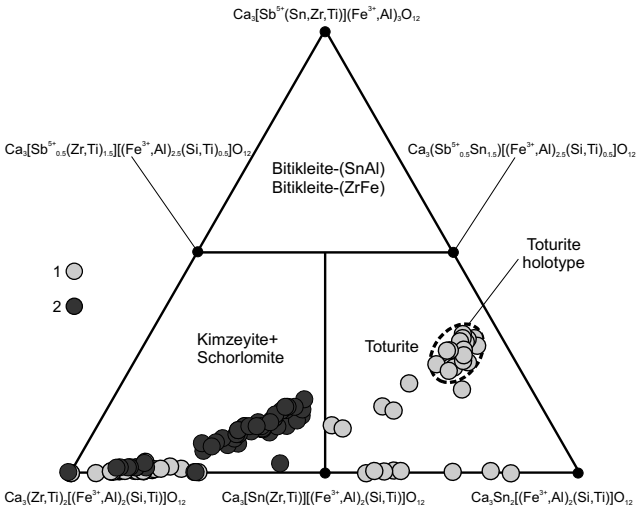

FIGURE 4. Compositions of garnet from the xenoliths plotted in terms of $Ca_3(Zr,Ti^{4+})_2[(Fe^{3+},Al)_2(Si,Ti^{4+})]O_{12}$ (kimzeyite-schorlomite type) – $Ca_3Sn_2[(Fe^{3+},Al)_2(Si,Ti^{4+})]O_{12}$ (toturite type) – $Ca_3[Sb^{5+}(Zr,Sn,Ti^{4+})](Fe^{3+},Al)_3O_{12}$ (bitikleite type): 1 = xenolith 3; 2 = xenolith 5.

Toturite crystallizes after kimzeyite (Fig. 1c), and the later appearance of thin zones of newly formed kimzeyite (Fig. 1b) is connected rather to the dissolution of the early Zr-minerals lakargiite and tazheranite. The simultaneous formation of the Sn-Zr-garnet, lakargiite, and a tazheranite-like phase, and the association with larnite, cuspidine, wadalite, and rondorfite, indicate a high temperature for metamorphism (Gazeev et al. 2006; Galuskin et al. 2009). Ignimbrite mafic minerals (micas, amphiboles, pyroxene) in which Sn usually disperses during the magmatic process were the likely source of the Sn.

ACKNOWLEDGMENTS

The authors thank to Associate Editor Ed Grew and reviewers Andrew Locock, Andrea Koziol, and Rachel Beane for their careful revisions that improved the early version of the manuscript. The work was partly supported by the Russian Foundation of Basic Researches, Project 08-05-00181. I.G. acknowledges support by the Ministry of Science and Higher Education of Poland, grant no. N307 097038.

REFERENCES CITED

Amthauer, G., McIver, J.R., and Viljoen, E.A. (1979) ^{57}Fe and ^{119}Sn Mössbauer studies of natural tin-bearing garnets. Physics and Chemistry of Minerals, 4, 235–244.

Belov, K.P. and Lyubutin, I.S. (1966) Effective magnetic fields at tin nuclei in substituted iron garnet $Ca_xY_{3-x}Sn_xFe_{5-x}$. Soviet Physics, 22, 518–520 (in Russian).

Butler, B.C.M. (1978) Tin-rich garnet, pyroxene, and spinel from a slag. Mineralogical Magazine, 41, 487–492.

Cartié, B., Archaimbault, F., Choisnet, J., Rulmont, A., Tarte, P., and Abs-Wurmbach, I. (1992) About the occurrence of tetrahedrally co-ordinated Sn^{4+} and Ti^{4+} in the new synthetic garnet-type solid solution $Ca_3Sn_{3-x}Ti_xFe_2O_{12}$ ($0.25 \leq x \leq 1.50$). Journal of Materials Science Letters, 11, 1163–1166.

Day, A. and Trimby, P. (2004) Channel 5 Manual HKL Technology Inc. Hobro, Denmark.

Galuskin, E.V., Gazeev, V.M., Armbruster, T., Zadov, A.E., Galuskina, I.O., Pertsev, N.N., Dzierżanowski, P., Kadiyski, M., Gurbanov, A.G., Wrzalik, R., and Winiarski, A. (2008) Lakargiite $CaZrO_3$: A new mineral of the perovskite group from the North Caucasus, Kabardino-Balkaria, Russia. American Mineralogist, 93, 1903–1910.

Galuskin, E.V., Gazeev, V.M., Lazic, B., Armbruster, T., Galuskina, I.O., Zadov, A.E., Pertsev, N.N., Wrzalik, R., Dzierzanowski, P., Gurbanov, A.G., and Bzowska, G. (2009) Chegemite $Ca_7(SiO_4)_3(OH)_2$—A new humite-group calcium mineral from the Northern Caucasus, Kabardino-Balkaria, Russia. European Journal of Mineralogy, 21, 1045–1059.

Galuskina, I.O., Galuskin, E.V., Dzierżanowski, P., Armbruster, T., and Kozanecki, M. (2005) A natural scandian garnet. American Mineralogist, 90, 1688–1692.

Galuskina, I.O., Lazic, B., Armbruster, T., Galuskin, E.V., Gazeev, V.M., Zadov, A.E., Pertsev, N.N., Jeżak, E., Wrzalik, R., and Gurbanov, A.G. (2009) Kumtyubeite $Ca_5(SiO_4)_2F_2$—A new calcium mineral of the humite group from Northern Caucasus, Kabardino-Balkaria, Russia. American Mineralogist, 94, 1361–1370.

Galuskina, I.O., Galuskin, E.V., Armbruster, T., Lazic, B., Dzierżanowski, P., Gazeev, V.M., Prusik, K., Pertsev, N.N., Winiarski, A., Zadov, A.E., Wrzalik, R., and Gurbanov, A.G. (2010a) Bitikleite-(SnAl) and bitikleite-(ZrFe)—New garnets from xenoliths of the Upper Chegem volcanic structure, Kabardino-Balkaria, Northern Caucasus, Russia. American Mineralogist, 95, 959–967.

Galuskina, I.O., Galuskin, E.V., Armbruster, T., Lazic, B., Kusz, J., Dzierżanowski, P., Gazeev, V.M., Pertsev, N.N., Prusik, K., Zadov, A.E., Winiarski, A., Wrzalik, R., and Gurbanov, A.G. (2010b) Elbrusite-(Zr)—A new uranian garnet from the Upper Chegem caldera, Kabardino-Balkaria, Northern Caucasus, Russia. American Mineralogist, 95, 1172–1181.

Gazeev, V.M., Zadov, A.E., Gurbanov, A.G., Pertsev, N.N., Mokhov, A.V., and

Dokuchaev, A.Ya. (2006) Rare minerals of Verkhniy Chegem caldera (in skarned carbonates xenoliths in ignimbrites). Vestnik Vladikavkazskogo Nauchnogo Tsentra, 6, 18–27 (in Russian).

Geller, S. (1967) Crystal chemistry of the garnets. Zeitschrift für Kristallographie, 125, 1–47.

Hatert, F. and Burke, E.A.J. (2008) The IMA–CNMNC dominant-constituent rule revisited and extended. Canadian Mineralogist, 46, 717–728.

Katerinopoulou, A., Katerinopoulos, A., Voudouris, P., Bieniok, A., Musso, M., and Amthauer, G. (2009) A multi-analytical study of the crystal structure of unusual Ti-Zr-Cr-rich andradite from the Maronia skarn, Rhodope massif, western Thrace, Greece. Mineralogy and Petrology, 95, 113–124.

Kononov, O.V., Evglevskaya, L.D., Klyuchareva, S.M., Korovkin, M.A., and Kabalov, Yu.K. (1989) Tin in garnet of the Tyrnyauz deposit. Doklady Akademii Nauk SSSR, 307, 1, 206–210 (in Russian).

Kraus, W. and Nolze, G. (1996) POWDER CELL—a program for the representation and manipulation of crystal structures and calculation of resulting X-ray powder patterns. Journal of Applied Crystallography, 29, 301–303.

Locock, A.J. (2008) An Excel spreadsheet to recast analyses of garnet into end-member components, and a synopsis of the crystal chemistry of natural silicate garnets. Computers and Geosciences, 34, 1769–1780.

McIver, J.R. and Mihálik, P. (1975) Stannian andradite from "Davib Ost," South West Africa. Canadian Mineralogist, 13, 217–221.

Milton, C., Ingram, B.L., and Blade, L.V. (1961) Kimzeyite, a zirconium garnet from Magnet Cove, Arkansas. American Mineralogist, 46, 533–548.

Mulholland, I.R. (1984) Malayaite and tin-bearing garnet from a skarn at Gumble, NSW, Australia. Mineralogical Magazine, 48, 27–30.

Munno, R., Rossi, G., and Tadini, C. (1980) Crystal chemistry of kimzeyite from Stromboli, Aeolian Islands, Italy. American Mineralogist, 65, 188–191.

Rulmont A., Tarte P., Cartié B., and Choisnet, J. (1993) Solid solutions $Ca_3Sn_{2+x}Si(Ge)_{1-x}Ga_2O_{12}$ ($0 \le x \le 0.95$) and tetrahedral coordination of Sn^{4+} in the garnet structure. Journal of Solid State Chemistry, 104, 165–176.

Rulmont, A., Tarte, P., Van Moer, A., Cartié, B., and Choisnet, J. (1995) Simultaneous occurrence of Sn^{4+} on the three cationic sites of the garnet structure: The solid solutions $Ca_xSn_xGa_{8-2x}O_{12}$ ($2.5 < x < 3.0$). Journal of Solid State Chemistry, 118, 6–9.

Schingaro, E., Scordari, F., Capitano, F., Parodi, G., Smith, D.S., and Mottana, A. (2001) Crystal chemistry of kimzeyite from Anguillara, Mts. Sabatini, Italy. European Journal of Mineralogy, 13, 749–759.

Scordari, F., Schingaro, E., and Pedrazzi, G. (1999) Crystal chemistry of melanites from Mt. Vulture (Southern Italy). European Journal of Mineralogy, 11, 855–869.

Shannon, R.D. (1976) Revised effective ionic radii and systematic studies of interatomic distances in halides and chalcogenides. Acta Crystallographica, A32, 751–767.

Sonnet, P.M. (1981) Burite, calcium hexahydroxostannate, a new mineral from El Hamman, Central Morocco. Canadian Mineralogist, 19, 397–401.

Strocka, B., Holst, P., and Tolksdorf, W. (1978) An empirical formula for the calculation of lattice constants of oxides garnets based on substituted yttrium- and gadolinium-iron garnets. Philips Journal of Research, 33, 186–202.

Whittle, K.R., Lumpkin, G.R., Berry, F.J., Oates, G., Smith, K.L., Yudintsev, S., and Zaluzec, N.J. (2007) The structure and ordering of zirconium and hafnium containing garnets studied by electron channeling, neutron diffraction and Mössbauer spectroscopy. Journal of Solid State Chemistry, 180, 785–791.

Wu, G. and Mu, B. (1986) The crystal chemistry and Mössbauer study of schorlomite. Physics and Chemistry of Minerals, 13, 198–205.

Zadov, A.E., Gazeev, V.M., Pertsev, N.N., Gurbanov, A.G., Yamnova, N.A., Gobechiya, E.R., and Chukanov, N.V. (2008) Discovery and investigation of a natural analog of calcio-olivine (γ-Ca_2SiO_4). Doklady Earth Sciences, 423A, 1431–1434.

MANUSCRIPT RECEIVED OCTOBER 14, 2009
MANUSCRIPT ACCEPTED APRIL 22, 2010
MANUSCRIPT HANDLED BY EDWARD GREW